공학박사학위논문

레이저 유도 종이 그래핀 기반 멀티모달 센서의 스마트 식품 관리로의 응용

Laser induced graphene-on-paper for multimodal sensor applications in smart food management

2023 년 8 월

서울대학교 대학원

기계공학부

민 진 기

레이저 유도 종이 그래핀 기반 멀티모달 센서의 스마트 식품 관리로의 응용

Laser induced graphene-on-paper for multimodal sensor applications in smart food management

지도교수 고 승 환

이 논문을 공학박사 학위논문으로 제출함

2023 년 4 월

서울대학교 대학원

기계공학부

민 진 기

민진기의 공학박사 학위논문을 인준함

2023 년 6 월

위 원 장 : 송한호 (인)

부위원장 : 고승환 (인)

위 원 : 박상욱 (인)

위 원 : 권진형 (인)

위 원 : 이진우 (인)

Abstract

With the global waste issue, including plastic waste and e-waste, becoming more severe, there is a growing need for greener materials in electronics. Thus, the use of green materials for food packaging and real-time monitoring of food quality is important for managing waste issues and human health. A state-of-the-art graphene synthesis method, laser-induced graphene (LIG), has been widely researched due to its excellent properties and feasibility of process. In this paper, we present a multimodal paper graphene sensor (MPGS) based on LIG-on-paper biodegradable substrates to develop next-gen green electronics. Direct irradiation of continuous wave laser successfully formed LIG on various paper substrates with decent sheet resistance of 105 Ω sq^{-1}. Also, the porous structure of LIG-on-paper made it sensitive to input signals, which is useful for sensor applications. Thus, LIG-on-paper is applied as a temperature-gas dual-mode sensor with sensitiveness of 0.15 % $°C^{-1}$ and 0.0041 % ppm^{-1} each, detecting both inputs by the single sensitive electrode. As a proof-of-concept, we developed the smart food management system that detects temperature of food and spoilage gas simultaneously. With the wireless communications of embedded processor, received data could be readily sent to mobile devices. We believe this paper-based electronics study will lead to the advancement of next-gen green electronics, addressing global waste and food safety issues.

Keyword : laser-induced graphene, multimodal paper graphene sensor, green materials, food spoilage, continuous wave laser, smart food management

Student Number : 2017-23145

Table of Contents

보존용 학위논문 정오표

페이지	정정 전	정정 후
p. 48 : 35	(43) Matindoust, S.; Farzi, A.; Nejad, M. B.; Abadi, M. H. S.; Zou, Z.; Zheng, L.-R. Ammonia gas sensor based on flexible polyaniline films for rapid detection of spoilage in protein-rich foods. 49 Journal of Materials Science: Materials in Electronics 2017, 28 (11), 7760-7768.	(43) Jung, Y.; Min, J.; Choi, J.; Bang, J.; Pyun, K.; Cho, Y.; Hong, S.; Hong, S.; Lee, J.; Ko, S.H. Smart Paper Electronics by Laser-induced Graphene for Biodegradable Real-time Food Spoilage Monitoring. Applied Materials Today 2022, 29, 101589.
p. 46 : 5	(2) The World Bank. WHAT A WASTE 2.0. https://datatopics.worldbank.org/what-a-waste/trends_in_solid_waste_management.html (accessed March 22, 2023).	(2) Min, J.; Jung, Y.; Ahn, J.; Lee, J.G.; Lee, J.; Ko, S.H. Recent Advances in Biodegradable Green Electronic Materials and Sensor Applications. Advanced Materials 2023, 202211273.

Chapter 1

Introduction

1.1 Motivation

As reported by the World Bank, global population growth and industrialization have resulted in a huge production of solid waste, reaching 2.24 billion tons in 2020, or 0.79 kg/person/day [1]. This problem is projected to increase and reach 3.88 billion tons by 2050. A considerable part of this waste, at least 23%, is non-biodegradable, with plastic as the dominant component [2]. Non-biodegradable waste poses a profound problem for disposal, as it does not degrade naturally and can only be landfilled, incinerated or recycled. Recycling, however, is unaffordable and inefficient. Furthermore, plastic production requires a lot of oil (4–8% of global consumption) and causes high C emissions [3]. Consequently, several governments have chosen to limit the use of non-biodegradable polymers such as plastics.

Garbage stockpile in Indonesia
(The Washington Post, 2017)

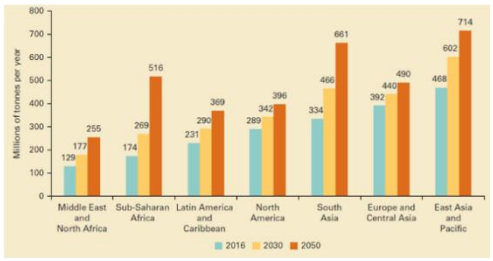

Projected waste generation by region (millions of tons/year)
(World Bank, 2018)

Figure 1.1: Pictures on global waste issue with generation rate by global regions [4] [2].

Novel electronics that use various non-biodegradable substances, such as printed circuit boards and semiconductors, have been developed as a result of the industrial revolution and its related technological progress. These electronic products generate a large amount of electronic waste ("e-waste") when they become obsolete. The Global E-waste Monitor reported that e-waste production reached 53.6 million tons in 2020 and is likely to grow to 74 million tons by 2030, with an average annual e-waste disposal rate of 4–5 kg/person [5]. In addition, e-waste disposal in landfills releases toxic gases, metals, and chemicals that pollute the soil and groundwater in the vicinity. The US Environmental Protection Agency has expressed concern about the negative impacts of e-waste on human health and the environment. Recycling has been suggested as a possible way to address these issues; however, it is not adequate as it primarily focuses on retrieving expensive metals. Thus, the demand for employing greener materials in electronics has emerged in recent decades.

E-waste stockpile
(Geneva Environment Network, 2023)

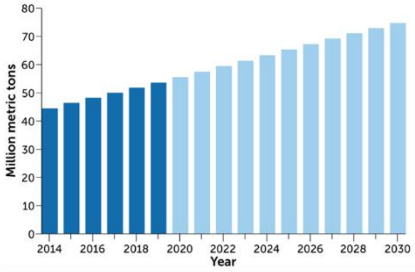

E-waste generation projectile
(ScienceNews, 2020)

Figure 1.2: Pictures on global e-waste issue with projected e-waste generation [6] [7].

Plastic waste, along with e-waste, has become a critical global issue. To reduce non-biodegradable plastic waste, many multinational franchise firms have started to replace typical plastic-based food-packaging materials with papers. To prevent food poisoning, it is important to monitor food status and use safe food packaging. In recent decades, food poisoning has affected approximately 600 million people and caused 420,000 deaths annually [8]. To reduce non-biodegradable plastic waste, many multinational franchise firms have started to replace typical plastic-based food-packaging materials with papers [9]. Real-time detectors for gas emission and temperature of the food products can minimize the risk of food poisoning because gas emission and temperature can determine the current food condition and further estimate the accurate shelf life of the food products. Most food products chemically decompose faster if they are not preserved at the proper temperature, and pathogen growth will start generating highly concentrated chemical gases in real-time as a result of organic decomposition [10] [11]. Therefore, it

is crucial to monitor food quality preserved in paper-based packages before consuming it because it eliminates the need to open the food package and manually check the spoilage level. A smart, real-time monitoring platform of food status will potentially benefit not only our daily life but also the storage and supply chains in the food industry.

1.2 Limitations of previous studies

There are prerequisites for effective food monitoring in daily life. The sensor must be directly integrated into the food package and should be made of biodegradable materials. However, most temperature or gas sensors are made of non-biodegradable materials such as conducting polymer, carbon nanotubes, and metal oxide [12]. These materials cannot be decomposed by natural species and pose a threat to global sustainability. Graphene, on the other hand, has desirable properties for temperature and gas sensing due to its outstanding electrical mobility and high surface-area-to-volume ratio [13] [14]. These properties facilitate the response to thermal energy and help the interaction with gas molecules [15]. Recently, several studies have utilized a cost-effective and facile laser patterning process for graphene formation by irradiating laser onto the polyimide (PI) to synthesize graphene [16] [17] [18] [19] [20]. This process is employed in various state-of-art flexible/wearable applications that include mechanical sensors [21] [22], chemical sensors [23], energy storage devices [24], energy harvesting devices, water splitting, and anti-bacterial air filter.

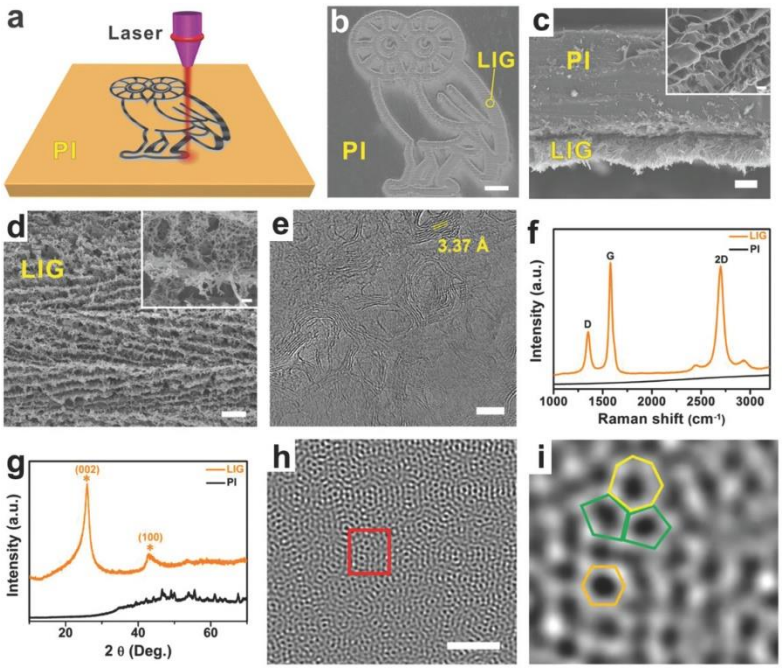

Figure 1.3: Laser-induced graphene (LIG) formation on polyimide (PI) [25].

Nevertheless, laser-induced graphene (LIG) on the PI film as a carbon precursor suffers from limitations to be applied on green electronics due to the intrinsically non-biodegradable nature of PI [26]. To address this issue, several research groups translated the LIG process to biodegradable substrates such as woods [25] and leaf [27, 28]. Out of many commercially available biodegradable substrates to derive LIG, the paper substrates provide several favorable properties for LIG formations. First of all, the papers originate from the natural elements, and thus they are completely biodegradable while exhibiting the highest recyclability among all the everyday solid waste [29]. In addition to its eco-friendly nature, the paper substrates also demonstrate high

flexibility, low cost, and ubiquity, offering desirable processibility for LIG. For this reason, a great number of researchers utilized papers to develop a myriad of cutting-edge technologies such as reusable transistors [30], memory device [31], energy harvesting device [32] [33], water splitting [34], biosensor [35], mechanical sensors [21] [22] and chemical sensor [23]. However, the direct derivation of LIG from the commercial thin paper (thickness ≈ 70 μm) involves practical limitations. Noticeably, it requires the additional process such as a chemical pretreatment on paper or high laser power with a pulsed beam that does not allow the LIG electrode to retain a stable structure on the paper substrate [37] [38]. In this regard, the visible continuous-wave laser serves as a viable candidate for LIG formation on the commercial paper as it can fabricate LIG with much lower power without damaging the entire substrate [22].

1.3 Preview of this study

In this study, we introduce a novel device called as multimodal paper graphene sensor (MPGS), designed for wireless monitoring of food status in everyday life. By utilizing continuous wave laser with low optical power (approximately 0.1 W), the laser irradiation process transforms various commercially available papers into LIG, without causing physical damage to the substrate, even without any prior chemical treatment. The ability to directly fabricate the MPGS on the paper-based packaging, without causing significant mechanical damage, presents a crucial advantage as it eliminates the need for a separate sensor fabrication process followed by integration into the food packaging materials. This simplified process, coupled with the all-in-one device/substrate architecture, indicates that simple laser irradiation on commercial papers enables food status monitoring.

Based on these advantages, we developed a paper circuit based on LIG that demonstrates high practical utility, as it can be easily shaped according to specific requirements. Additionally, the inflammable nature of paper allows for secure handling of classified circuit information without the need for complex encryption processes, as it can simply be incinerated. Moreover, the patterned LIG exhibits a favorable sheet resistance (105 Ω sq-1), enabling precise detection of temperature and trimethylamine (TMA) gas, which is produced during the decomposition of

protein-rich foods. The dual functionality of the LIPS as both a temperature and chemical sensor enables the monitoring of food spoilage. The detection of TMA, which is directly related to food freshness, allows for an assessment of the food's condition, while the temperature measurement provides information on how the food's state may change over time.

Chapter 2

Methods

2.1 Optical setup and LIG synthesis method

To create graphene on different paper materials, a continuous-wave laser with a wavelength of 532 nm and made by Lighthouse Photonics Inc. was used. The laser beam was directed through an optical system that has a galvano-mirror scanner system equipped with a telecentric lens. A galvano-mirror scanner is a device that employs a mirror galvanometer. In a mirror galvanometer, an electric current moves a mirror and a light beam is reflected by the mirror onto a scale. The greater the current, the greater the deflection of the light beam. Galvanometer scanners utilize this technology of moving a mirror with an electric current to reflect and direct a laser beam. The galvano-mirror scanner was linked to a computer-aided patterning software that is able to manage the laser power, scanning speed, and CAD design for creating specific patterns. Using this patterning system, various types of commercial papers, including colored paper, paper cups, and milk cartons, were exposed to the laser beam and were transformed into LIG.

2.2 Material Characterization

The FE-SEM (SUPRA 55VP; ZEISS) was utilized to analyze the surface and cross-sectional morphology. In order to measure the molecular fingerprint, Raman spectroscopy was performed using the Raman microscope (inVia Raman microscope; Renishaw) as shown in **Figure 3.2b**. The Raman spectrum displayed the measured Raman spectrum where the D band (≈ 1340 cm^{-1}), G band (≈ 1585 cm^{-1}), and 2D band (≈ 2675 cm^{-1}) were all clearly detected. The D band indicated bent sp^2 carbon bonds or other defects, the G band shows first-order Raman scatttering, and the 2D band indicated by second-order zone-boundary phonons [26]. The weak peak of the 2D band indicated the formation of multilayer LIG ($I_{2D}/I_G > 2$ for single-layer graphene). The 2D band was redshifted by around 10 cm^{-1} compared to that of ideal graphene (≈ 2685 cm^{-1}) due to the stretching of the carbon-carbon bond of graphene, which is subjected to tensile strain because of the rapid heating process during laser irradiation [36] [37]. The D+D′ band (≈ 2904 cm^{-1}) showed defects in the material [38]. The quality of LIG was also examined by using X-Ray Diffractometer (D8-Advance; BRUKER MILLER Co.) and X-ray photoelectron spectroscopy (AXIS-HSi; Kratos). The XRD spectrum (**Figure 3.2c**) exhibited the peak at $2\theta = 28°$ with (002) plane, which indicated the formation of multilayer graphene [39]. In the XPS spectrum (**Figure 3.2d**), three peaks were observed at a binding energy of 284.7 eV, 286 eV, and 288 eV, and each peak signified sp^2, C-O, and C=C bondings respectively [27] [40] [41]. The most dominant peak at 284.7 eV verified the

presence of graphene [42]. By conducting molecular footprint analysis through three methods, we were able to determine that graphene was successfully formed on ordinary paper via laser processing.

2.3 Functionality experiment of Multimodal Paper Graphene Sensor (MPGS) as multimodal sensor

The evaluation of MPGS response to temperature was carried out on commercial TEDs, which were used to regulate temperature by altering the direction and intensity of the electrical current in the surrounding environment. To heat up the TEDs, we gradually increased the electrical current input. On the other hand, for the cooling mode, the same procedure was followed, but with the electrical current flowing in the opposite direction. We monitored the real-time response of MPGS at different temperatures while simultaneously recording the temperature of TEDs. The MPGS was not enclosed during the temperature sensing test.

To introduce a specific amount of gas to the sensor, a custom-built gas chamber was utilized. Two mass flow controllers (MFCs) were employed to regulate the gas flow rate of TMA gas and N_2 gas (**Figure 2.1**). At room temperature, the MPGS was placed inside the gas chamber (**Figure 2.2**). For each TMA concentration, a fixed amount of N_2 gas was mixed with a certain flow rate

of TMA gas. To assess the MPGS' reproducibility in TMA sensing, the TMA gas valve was closed when the resistance change peaked, while the N_2 gas continued to flow to lower the TMA concentration. A source meter (Keithley Instruments, Model 2400) was linked to the MPGS and computer, equipped with custom-designed software to continuously monitor changes in sensor resistance. The data for measuring MPGS's response time to various TMA concentrations, was filtered and calibrated using a simple baseline manipulation to minimize the baseline drift that occurs naturally due to TMA molecules that are not desorbed from the MPGS during the recovery period. The MPGS was not enclosed during the gas sensing test.

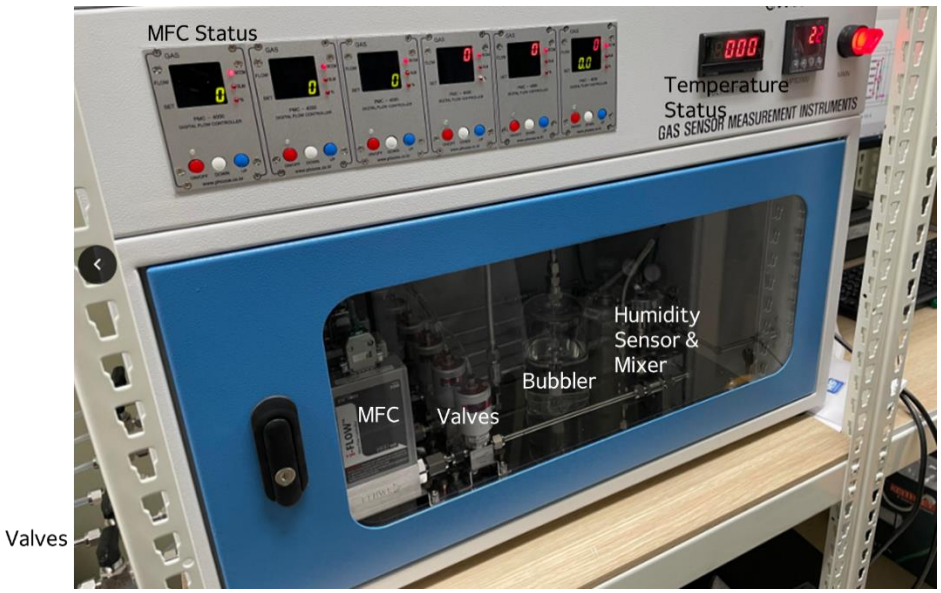

Figure 2.1: Overall image of the gas sensing system with MFCs

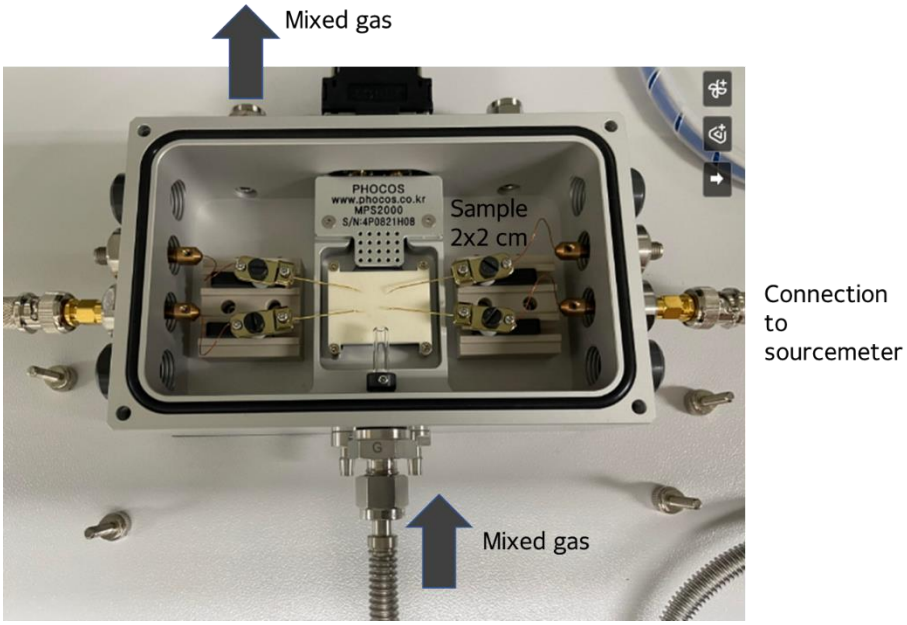

Figure 2.2: Optical image of gas sensing chamber

2.4 Real-life application methods for MPGS

To monitor food spoilage, we utilized a microcontroller based on Tensilica Xtensa LX6 microprocessor (ESP32; Espressif Systems) and an antenna-embedded board for wireless communication with the server. The resistance variance was measured through a voltage-dividing method applied to MPGS, and the signal was quantified via a built-in analog-to-digital converter of the MCU. The MCU was programmed to transmit the data received through WiFi to a designated web server. We sensed the spoilage of 176 g of raw pork meat placed inside a 750 mL air-tight plastic chamber stored under control thermal conditions (4 ˚C) and at 37 ˚C in the oven. To fabricate MPGS on the milk carton, we disassembled it and patterned MPGS on the inner

surface, then resealed it by sticking adhesives on the disassembled part. Two sets of 200 mL of milk were kept at 4 ˚C (fresh) and 37 ˚C (spoiled), respectively, and monitored using the same procedure over time. MPGS was fabricated on the inner side of the milk carton facing inside to monitor milk spoilage.

Chapter 3

Synthesis and optimization of LIG

3.1 Overview of the study

The depiction in **Figure 3.1** illustrates a process of photothermal pyrolysis achieved by using a continuous-wave laser to generate porous LIG from paper without damaging the paper substrate. This method of laser patterning on commercial paper can be easily used to create MPGS for in-situ fabrication of sensors on everyday items like milk cartons and paper cups, which can then be used to monitor the chemical and thermal status of food products. This provides a distinct advantage in terms of the fabrication process as compared to previous sensors, which had to be integrated into the packaging substrate after fabrication [43]. By fabricating MPGS on the inner surface of a milk carton, TMA gas produced from protein-rich foods during organic decomposition can be detected to monitor the freshness of the milk inside the carton. Moreover, laser irradiation on the outer surface of a paper cup can enable the MPGS to detect the temperature of the water inside, providing a practical food monitoring platform that can detect food conditions in real-time and the near future. The TMA sensing capability of MPGS allows for the monitoring of current food freshness, while temperature delivers information on whether products are preserved in a proper thermal condition, providing expected information about the future food status.

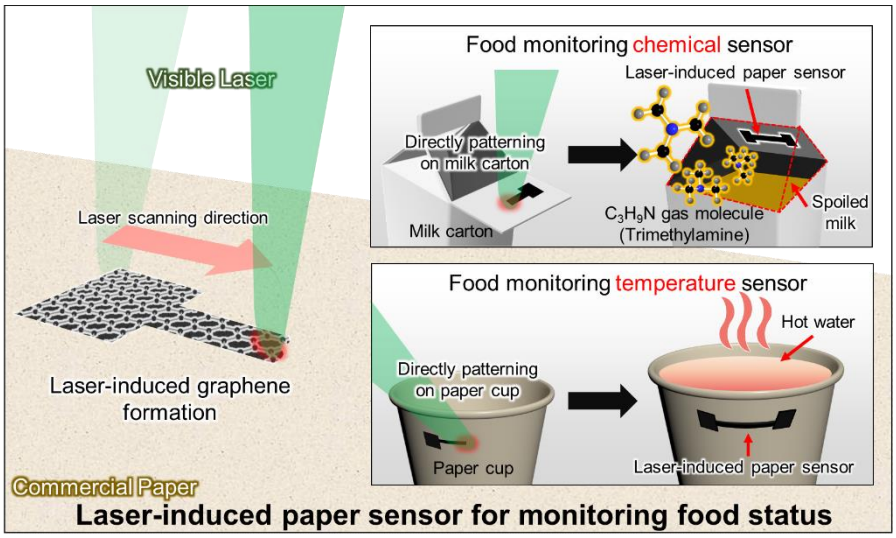

Figure 3.1: Overall schematics of MPGS fabrication process and applications

By using continuous-wave laser irradiation on commercial papers such as milk cartons, paper cups, colored paper, and paper bags, LIG can be produced (**Figure 3.2a** and **3.3**). SEM imaging of magnified views on colored paper reveals that laser irradiation on a paper substrate generates a porous graphene structure. This porosity of the graphene electrode allows for high sensitivity gas sensing due to the high surface-to-volume ratio of the porous structure. Chemical analysis of LIG can be obtained through Raman spectroscopy, X-ray diffraction (XRD), and X-ray photoelectron spectroscopy (XPS) (**Figure 3.2b-d**, refer to the Methods Section for more details).

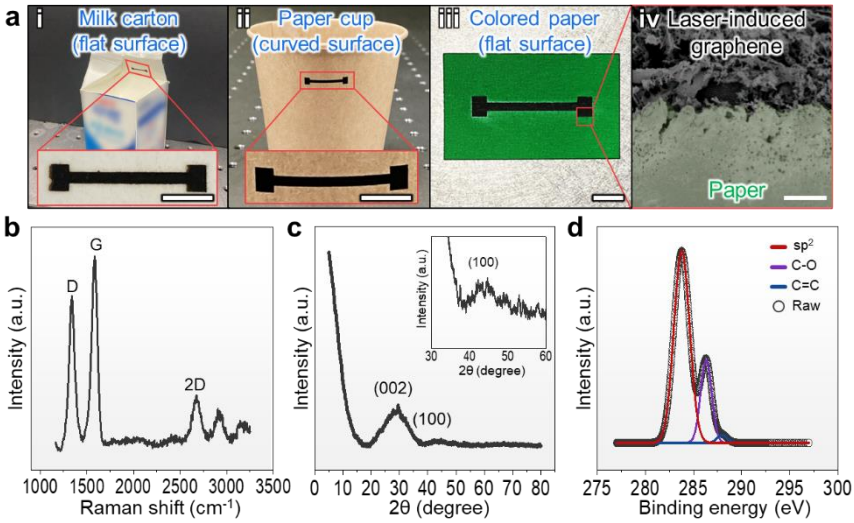

Figure 3.2: a) The photographs of laser-induced graphene (LIG) patterned on commercial milk carton, paper cup, and colored paper are shown with scale bars of 5 mm, along with a scanning electron microscope (SEM) image of LIG on colored paper with a scale bar of 10 μm. b) The Raman spectra of LIG are presented. c) The X-ray diffraction (XRD) spectra of LIG are shown. d) The X-ray photoelectron spectroscopy (XPS) spectra at C 1s of LIG are presented.

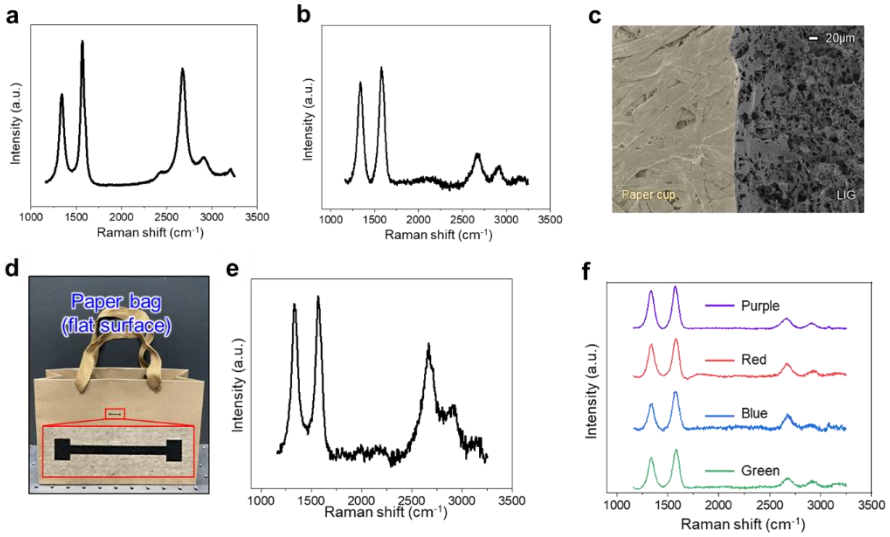

Figure 3.3: a) Raman spectra of LIG on inner surface of milk cartoon. High 2D peak (I_{2D}/I_G = 0.8) is observed, which implicates thin layer of graphene. b) Raman spectra of LIG on paper cup. c) The SEM image of LIG on paper cup. d) Optical image of LIG on paper bag. e) Raman spectra of LIG on paper bag. f) Raman spectra of LIG on various colored origami paper.

3.2 Optimization for LIG fabrication process

To fabricate MPGS for monitoring food status, obtaining high-quality LIG is crucial. Therefore, we investigated the impact of laser irradiation on LIG formation and optimized the fabrication process to produce both mechanically and electrically stable LIG. **Figure 3.4a** presents the image of the as-fabricated LIG samples (4 cm × 4 cm) generated by varying laser power and scan rate. High laser power and low scan rate conditions resulted in high laser energy density (as $\delta \approx \frac{p}{v}$,

where p is the laser optical power, and v is the scanning speed) [44], leading to damage of the paper substrate (blue zone). However, low energy density conditions failed to promote LIG formation, resulting in partially patterned regions (black zone). This suggests that delivering an appropriate amount of localized photonic energy is crucial for producing high-quality graphene. The laser-pyrolyzed samples in the whole-patterned region (red zone) remained intact, and we conducted further characterization only on these samples. To assess the electrical properties of LIG, we measured electrical resistance for various parametric conditions, as shown in **Figure 3.4b**. **Figure 3.5** indicates that electrical conductivity tends to improve with increasing laser energy density within the laser-pyrolyzed samples. Thus, we obtained a relatively low sheet resistance of 105 Ω sq^{-1} at a laser power of 100 mW and a scan rate of 10 mm/s. More details on the characterization and fabrication process can be found in the Methods Section.

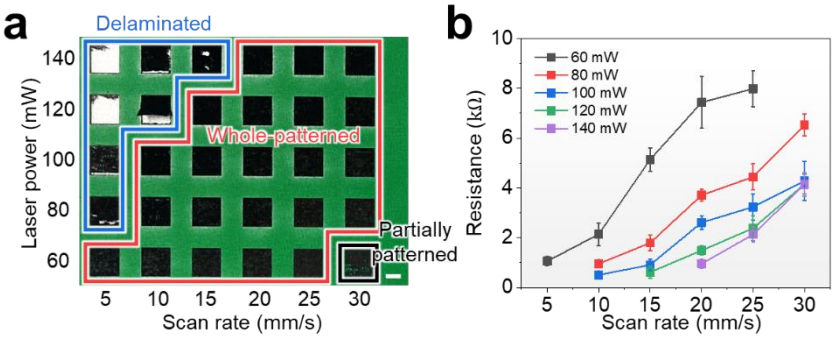

Figure 3.4: Optimization of process parameters for LIG formation. a) Applying various laser processing conditions regarding laser powers (60 ~ 140 mW) and scan rate (5 ~ 30 mm/s). The delaminated, whole-patterned, and partially patterned regions are highlighted as blue, red, and black zone, respectively (scale bar: 2 mm). b) The resistance of LIG at different scan rates and laser powers.

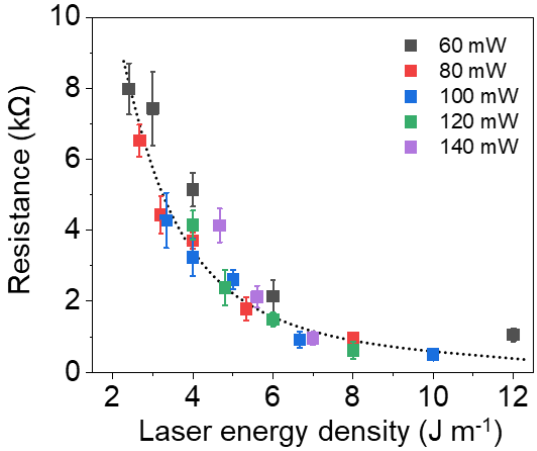

Figure 3.5: Distribution of green origami paper LIG resistance in various laser energy density (hatch distance: 15 µm).

We used Raman spectroscopy to examine laser-pyrolyzed samples that were exposed to various laser powers at a fixed scan rate of 20 mm/s, in addition to performing electrical characterization (**Figure 3.6a**). The Raman spectra indicated a clear 2D peak at a laser power of 100 mW, demonstrating second-order scattering and confirming the synthesis of multilayer graphene from paper substrates through laser irradiation instead of amorphous carbon [45] [46]. Based on these properties, we studied the respective thicknesses of the LIG layer and substrate by analyzing cross-sectional SEM images at various scan rates with a fixed laser power of 100 mW to determine the optimized conditions for producing mechanically and electrically stable LIG on top of the free-standing paper substrate (**Figure 3.6b**). A lower scan rate results in a higher LIG thickness, which can provide a greater number of electrically conductive paths, but there is a clear trade-off between the conductive path and substrate thickness. The high laser energy density transforms a significant portion of the cross-sectional paper substrate into LIG, rendering the whole LIG/paper structure mechanically unstable. For instance, an extremely low laser scan rate (5 mm/s) severely damages the paper substrate to the point where the resulting material is not only electrically but also mechanically disconnected, as observed in the samples shown in **Figure 3.4a** and **b**. However, laser irradiation with optimized laser parameters (v = 10 ~ 20 mm/s) on the thin commercial paper converts only a desirable cross-sectional portion of the paper into high-quality LIG without harming the substrate. This hybrid all-in-one structure makes it easier to apply MPGS to food

packaging materials since LIG on a free-standing paper substrate can monitor food status without the need for an additional fabrication process to transfer laser-induced graphene to another substrate.

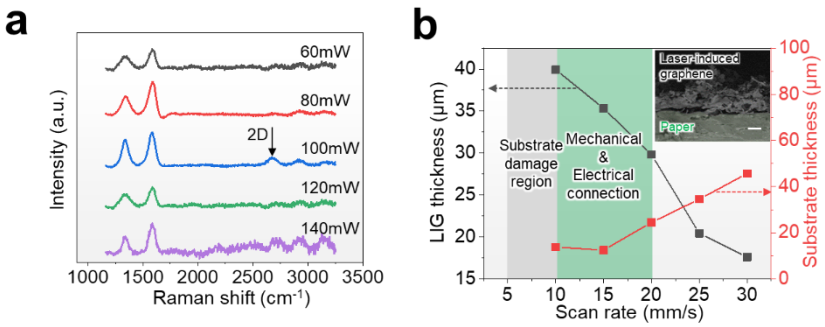

Figure 3.6: a) Raman spectra of LIG were obtained at different laser powers (60 ~ 140 mW) with a fixed scan rate of 20 mm/s. b) The thickness of LIG layer and substrate layer were measured at different scan rates with a fixed laser power of 100 mW. The inset shows a cross-section view of the SEM image (scale bar: 10 μm).

One of the most intriguing aspects of laser processing is its ability to manipulate the focal point of the laser beam on a paper substrate to create the laser-induced graphene (LIG) structure with varying resolutions. By controlling the laser focal point, we can switch between localized and large-area patterning modes depending on the intended fabrication purpose. In order to evaluate

the quality of LIG at different defocusing levels, we varied the focal points from 0 (high-resolution patterning) to 0.8 mm (large-area patterning), as shown in **Figure 3.7a** and **b**. For the defocused mode, we used higher laser power to maintain the average photonic intensity per area. The results showed that the line width of LIG was 13.1 μm when irradiated at the focal point (0 mm), and it increased as the defocusing level increased. At a defocused level of 0.8 mm, we obtained a greater line width of 34.71 μm, indicating that defocused laser processing can shorten the processing time required to scan an arbitrary area of the paper substrate.

Despite the clear advantage of reducing processing time, the LIG quality did not suffer when using the defocused laser mode. **Figure 3.7b** demonstrates the chemical structure of LIG based on I_D/I_G and I_{2D}/I_G ratios, which showed a consistent quality of LIG regardless of the laser focal point. A lower I_D/I_G ratio implies higher surface quality, and a higher I_{2D}/I_G ratio suggests a high proportion of LIG remains as single-layer graphene [47]. This indicates that both I_D/I_G and I_{2D}/I_G ratios remained constant even at the greatest defocusing level. This feature of LIG offers design freedom, as we can use high-resolution patterning to micro-pattern the electrode and switch to the defocusing mode for large-area fabrication, depending on the specific design purpose.

Table 1 compares the quality of MPGS with that of previous works based on the origin of graphene and sheet resistance. As shown in the table, the sheet resistance of MPGS was 105 Ω/sq, falling within the reasonable range of sheet resistance of polyimide-based LIG. The sheet

resistance of LIG can vary depending on the average thickness of the LIG electrode. For example, MPGS has a relatively thin thickness of 39.9 μm, while LIG in another work with the sheet resistance of 30 Ω/sq had a greater thickness of 100 μm [48]. This demonstrates that the sheet resistance of LIG is inversely correlated with its thickness since thicker LIG provides a greater number of conductive paths for electron transfer. However, we intentionally optimized the thickness of LIG to maintain a stable structure of LIG sensor on the free-standing paper substrate, despite a trade-off of electrical conductivity. The free-standing paper-based structure eliminates the need for the additional process of transferring LIG to another substrate, and such a hybrid structure of sensor and paper substrate utilizes the LIG sensor without any modification.

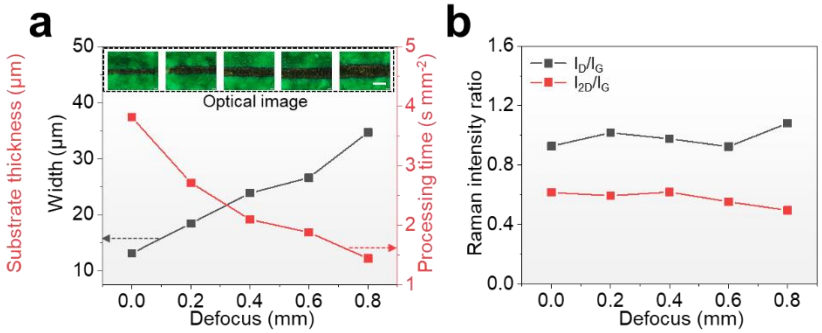

Figure 3.7: a) The width of LIG lines and the time required for their formation depend on the defocus level used during laser irradiation, which varies from 0 to 0.8 mm. A photograph in the inset displays the width of LIG lines created at different defocus levels, with a scale bar of 30 μm. b) The intensity ratios of ID to IG and I2D to IG in LIG are influenced by the defocus level used during laser irradiation.

Reference	Graphene origin	Sheet resistance (Ω/sq)	Application
[48]	Polyimide	30	Chemical sensor
[49]	Polyimide	78	Gas sensor
[50]	Wood	1500	Supercapacitor
[51]	Polyimide	20	Heater, surface treatment
[19]	Polyimide, cork	120	Triboelectric nanogenerators
[52]	Polypropylene	130	Triboelectric, surface treatment
[53]	Polyimide	5 - 20	Bacterial air filter
[54]	Polyimide	108	Humidity sensor
[55]	Polyimide	15,000	Chemical sensor
[40]	Cloth, paper, food	15	Electrode
[56]	Polybenzoxazine resin	35	Supercapacitor
[57]	Phenolic resin	44	Supercapacitor
[58]	Wood	7	Electrocatalysis, EMI shielding
[59]	Polyimide	250	Heater
[60]	Polyimide	300	Surface treatment
This work	**Paper**	**105**	**Gas sensor/temperature sensor**

Table 1: Comparison of MPGS from various researches

In addition to analyzing the chemical properties of the paper-based LIG, we conducted a bending test to confirm its mechanical durability. As the connection between the LIG electrode and electrical wires is vulnerable to mechanical stress, we utilized EGaIn to connect the wire to the LIG electrode and sealed it to prevent leakage, as depicted in **Figure 3.8a**. We measured the normalized resistance as the bending radius decreased to assess the mechanical stability of the LIG electrode, and found that it can withstand bending radii of up to 2.5 mm, as shown in **Figure**

3.8b. Moreover, we observed consistent resistance change over 1000 cycles of bending with a bending radius of 3.1 mm, as depicted in **Figure 3.8c**. The LIG electrode's mechanical robustness and resistance to fatigue stress indicate that the MPGS can transmit food spoilage data to the end-user while enduring everyday mechanical stress.

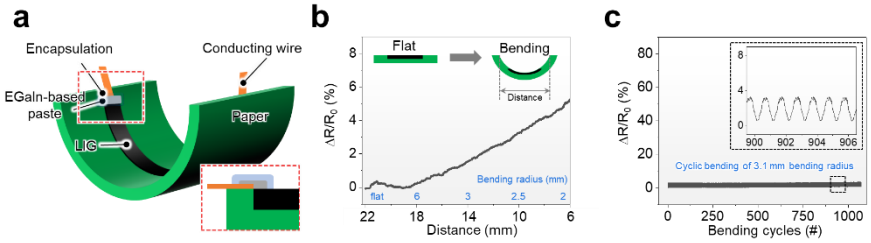

Figure 3.8: a) The visual depiction of the experimental arrangement used for the cyclic bending test. b) The alteration in resistance of the LIG electrode corresponding to the variation in the bending radius. c) The modification in resistance of the LIG electrode during the cyclic bending test.

3.3 Utilization of LIG as green circuit

Utilizing paper as a medium to create graphene provides several distinctive advantages when using LIG as an electrical circuit. One of the benefits is the capability to effortlessly pattern a LIG-based paper circuit on both surfaces of a flat colored paper and curvilinear paper cup. Moreover, the LIG circuit can be cut into any desirable shape, eliminating the need for a

conventional dicing or cutting process (**Figure 3.9a**). Along with the tailorable nature of the paper-based LIG circuit, we also demonstrated that the circuit can activate red, yellow, and green light-emitting diodes (LEDs) when a DC voltage was applied to the circuit due to its exceptional electrical conductivity (**Figure 3.9b**). The circuit's easily disposable nature is also noteworthy, as it can catch fire and burn into waste as shown in **Figure 3.9c**. This feature could potentially secure the confidential information of the circuit without a complex encryption process.

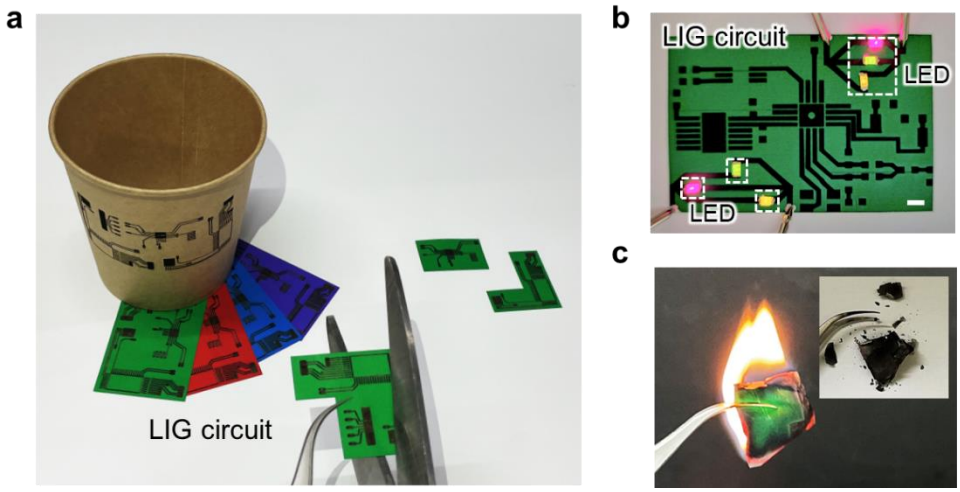

Figure 3.9: Utilization of LIG as green circuit. a) The LIG circuit can be created on both flat colored paper and curved paper cups. Moreover, it can be conveniently trimmed using scissors. b) We exhibited a demonstration of the LIG circuit that included a patterned circuit on the paper, along with red, yellow, and green LEDs (5mm scale bar). When we applied a DC voltage to the circuit, the LEDs illuminated.

Chapter 4

Characterizations of MPGS

4.1 Evaluation of MPGS as temperature sensor

We first tested how MPGS responded to temperature and TMA gas on colored paper before verifying its potential for monitoring food status. Temperature and spoiled gas emissions are indicators of food status, as improper thermal conditions can cause food to decompose and generate organic gases over time. To assess MPGS' temperature sensing capabilities, we measured its electrical resistance response on colored paper to temperatures ranging from 50 to 60 ˚C under both cooling and heating modes using a commercial thermoelectric device (TED). **Figure 4.1a** displays the temperature-dependent resistance profile of MPGS within the given temperature range, with room temperature (≈ 21 ˚C) as a reference value according to resistance. Additionally, **Figure 4.1b** shows that MPGS responds quickly to temperature changes by presenting the real-time temperature of the heat source on which it was mounted. Apart from its response to temperature changes, MPGS also exhibits a negative temperature coefficient of resistance (TCR) of -0.15 %/˚C (**Figure 4.1c**), which is comparable to that of previous carbon-based temperature sensors, as outlined in **Table 2**. Furthermore, according to Figure S6, the type of paper used does

not affect MPGS' temperature sensing performance, as MPGS on a paper cup shows a TCR value comparable to that of the colored paper.

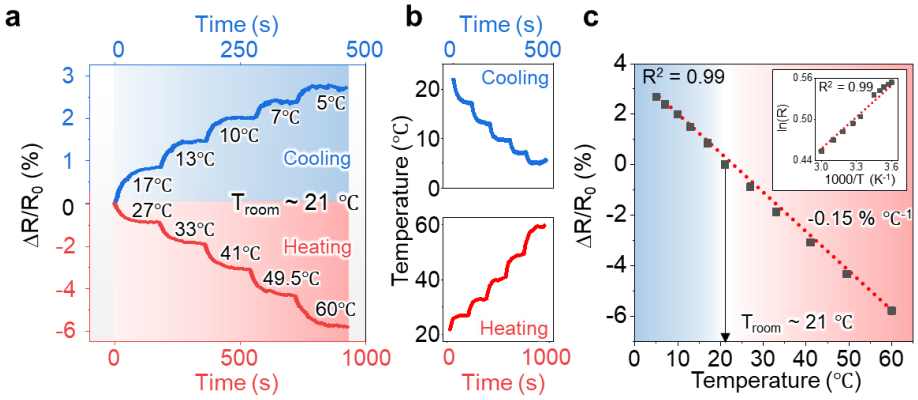

Figure 4.1: Evaluation of MPGS as temperature sensor. a) The instantaneous reaction of MPGS to temperatures ranging from 5 ˚C to 60 ˚C. b) The present temperature of MPGS: the upper and lower graphs illustrate the temperature of MPGS on the thermoelectric device during cooling and heating mode, correspondingly. c) Variation in response according to temperature, displaying negative temperature coefficient characteristics. The inset graph demonstrates the dependency of the natural logarithm of the resistance (ln(R)) on the reciprocal of the temperature (1/T).

Reference	Material	Temperature range (℃)	Temperature coefficient of resistance (% ℃$^{-1}$)
[61]	Carbon-graphene hybrid	30 – 45	-0.0017
[62]	Carbon black aerosol	25 – 85	0.13 - 0.15
[27]	LIG on leaf	20 -60	-0.08
[63]	Graphite on paper	27 – 107	-0.29
[64]	Graphene flakes	25 – 150	-0.18
[65]	Carbon black foam	25 – 70	0.19
[66]	NiO	25 – 70	-0.4
[67]	Ag	30 – 40	0.5
This work	LIG on paper	15 – 60	-0.15

Table 2: Comparison of MPGS temperature sensibility to recent works.

4.2 Evaluation of MPGS as amine gas sensor

We investigated how MPGS responds to TMA gas at room temperature, aiming to replicate the conditions of monitoring food freshness in daily life. TMA gas is an ideal indicator of food freshness since protein-rich food products generate TMA in a gaseous state during organic decomposition. Typically, gas sensors employ separate heaters to enhance gas sensing performance such as sensitivity and cyclic stability, and some have self-heating capabilities based on Joule heating, which generates heat by applying electrical voltage to the conductor. However, we chose not to use such measures to create a more realistic environment for our experiments.

When TMA gas molecules attach to the three-dimensional (3D) porous structure of LIG on commercial paper, they act as electron donors, causing the resistance of MPGS to increase as electrons recombine with the holes on graphene. This allows for the direct detection of food freshness. Before analyzing the gas sensing performance of MPGS, we conducted gas sensing tests with LIG fabricated using varying laser energy densities to optimize TMA sensing capability. **Figure 4.2a** shows the different LIG samples we used. Our results indicated that there is an optimal condition for MPGS fabrication, as it leads to a much more stable gas sensitivity performance. MPGS fabricated with low energy density had slower response times compared to those fabricated with optimal energy density, while MPGS fabricated with high energy density demonstrated unstable and fluctuating gas performance that could deliver inaccurate information to end-users.

The results of **Figure 4.3a** show the gas-sensing performance of MPGS for various concentrations of TMA gas, ranging from 5 to 40 ppm. Starting from the detection limit of 5 ppm, MPGS demonstrated an increase in resistance response with increasing TMA concentrations of 5, 10, 20, and 40 ppm, which is due to the adsorption of TMA molecules on the LIG surface as donors. This shows that the sensitivity of MPGS has a positive linear correlation with TMA concentrations. When compared with other gas sensors previously reported in **Table 3**, MPGS exhibits comparable performance to state-of-the-art gas sensors, with a limit of detection of 5

ppm, falling within the range of most state-of-the-art gas sensors. However, MPGS has a relatively longer response and recovery time (51.5 s and 65.9 s, respectively) compared to some gas sensors that have embedded heaters, which can accelerate the absorption and desorption of target molecules, and respond and recover within a few seconds. Nonetheless, MPGS still shows faster response and recovery times than other sensors that operate at room temperature, which can take hundreds of seconds to respond and recover (as shown in **Figure 4.2b**). To avoid safety issues and manufacturing cost, we did not include a heater in the food status monitoring system as it would involve a heater, power source, and other electrical components. Also, since the LIG gas sensor is directly applied to food packaging, incorporating a heater could pose a potential safety risk.

The MPGS system is capable of detecting the level of food spoilage due to its low detection limit of 5 ppm for TMA gas, which is considered fresh for meat and fish according to previous reports and Occupational Safety and Health Administration standards. The article also indicates that TMA concentration ranging from 10 to 50 ppm signifies the initial stage of organic corruption, while a concentration greater than 60 ppm indicates that the food is rotten and inedible, making it possible to determine whether food is still safe to eat through real-time monitoring of TMA using MPGS. In addition, the gas coefficient of resistance for MPGS was found to be 0.0041 % ppm-1, which is significantly different from the temperature coefficient of resistance, indicating

that the two sensing targets can be decoupled. To test the reproducibility of MPGS, a cyclic test was conducted by periodically exposing MPGS to TMA gas of a constant concentration of 40 ppm for a consistent time period, and the results showed moderately consistent responses with the constant concentration of TMA gas. **Figure 4.3c** also shows the consistent response change of TMA sensing performance of MPGS over several days, as MPGS was exposed to 40 ppm of TMA over 7 days, and the response change remained highly consistent for each day, indicating the reliable consistency of MPGS.

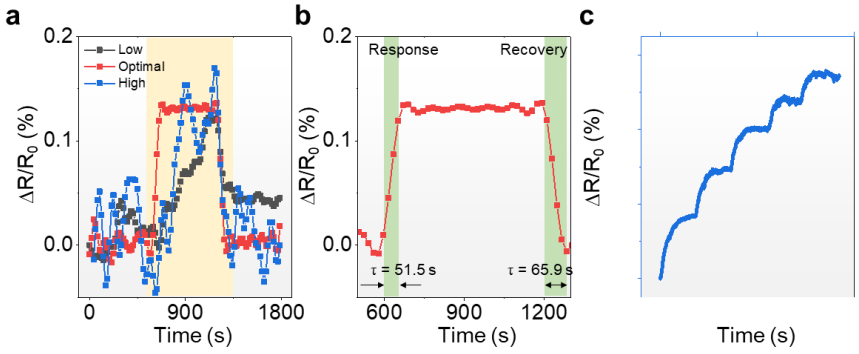

Figure 4.2: Evaluation of MPGS as amine gas sensor. a) The MPGS made with different laser energy density were tested for their real-time response to a fixed concentration of TMA gas at 40 ppm. The laser energy densities used were high (9 J m-1), optimal (8 J m-1), and low (7 J m-1). b) Figure 1g was magnified to observe the response and recovery of the MPGS more closely. c) The real-time repeatability

of MPGS to 40 ppm TMA gas was tested at room temperature to determine the consistency of its response over time.

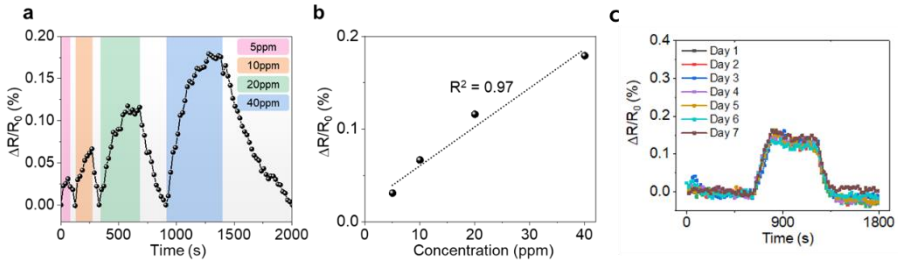

Figure 4.3: a) To determine the real-time response of MPGS, the system was exposed to different concentrations of TMA gas ranging from 5 to 40 ppm at room temperature. The response variation was measured and plotted as a function of TMA concentration, showing a positive linear relationship. However, it's important to note that the data was filtered and calibrated using a simple baseline manipulation technique to minimize the baseline drift. This is necessary due to the TMA molecules that remain on the MPGS during the recovery period, which can cause natural baseline drift. b) Shows the response variation in detail. c) The performance of TMA sensing was repeated over seven days.

Reference	Material	Substrate	Target gas	Limitation of detection (ppm)	Operating temperature (℃)	Response/ recovery time (s)
[68]	CVD grown graphene	Polyethersulfone	NO_2	500	250	26/480
[69]	PeDOT:PSS-graphene	Paper	NH_3	10	25 (RT)	N/A
[70]	CVD MOS_2	Polyimide	NO_2	25	25 (RT)	180/489
[71]	ZnO nanoflower	Polyimide	NO_2	50	270	25/14
[72]	MoS_2	PET	NO_2	1.2	N/A	1800/1800
[18]	LIG	PI	CO_2	100	N/A	8/25
[73]	SnO_2 NPs	SiO2/Si (not flexible)	H_2	1	50	1.1/1.1
[74]	SnO_2/graphene	SiO_2	NO_2	1	150	129/107
[75]	Ag-NA-rGO	N/A	NO_2	1	25 (RT)	600/2400
[76]	Functionalized rGO	Free-standing	Ethanol, acetone	25	N/A	40/260
[77]	MoS_2/graphene aerogel	Si substrate	NO_2	0.05	200	21/29
[78]	Polypyrrole /Graphene	Nylon membrane	NH_3	0.2	25 (RT)	300/600
[79]	rGO/PANI	Cotton	NH_3	0.4	25 (RT)	219/541
[80]	Functionalized graphene	SiO_2	NH_3	1.6	25 (RT)	900/NA
This work	LIG	Paper	TMA	5	25 (RT)	51.5/65.9

Table 3: Comparison of gas sensing ability to recent works

Chapter 5

Real-life applications of MPGS

5.1 MPGS as beverage thermal sensor in real-life scenario

To validate the practical application of in-situ fabricated MPGS on commercial papers for monitoring food status in daily life, various experiments were conducted to detect the thermo- and chemical-status of food, as shown in **Figure 5.1** and **5.2**. The first experiment was aimed to monitor the thermo-status of food by pouring hot and cold water into a commercial paper cup and then draining it. The temperature-dependent resistance profile of MPGS on the outer surface of the paper cup was used to detect the water temperature in different situations, as depicted in **Figure 5.1**. The MPGS initially showed no resistance change when there was no water in the cup, but the resistance started to drop immediately after pouring hot water (around 80 ˚C) into the cup. As the water cooled down (approximately 55 ˚C), the resistance gradually approached its original value due to heat exchange with the surrounding air. However, draining the water resulted in a sharp increase in resistance change, which returned to its original state after a short period. The same experiment was repeated with ice water, and the resistance of the sensor increased rapidly, plateaued for a while, and dropped back to its original value as the water was poured off the paper cup. In the case of cold water, the sensor resistance remained relatively constant over time because the temperature of the ice water did not change. It is noteworthy that the data was filtered and

calibrated using simple-baseline manipulation to minimize baseline drift caused by TMA molecules that were not desorbed from the MPGS during the recovery period.

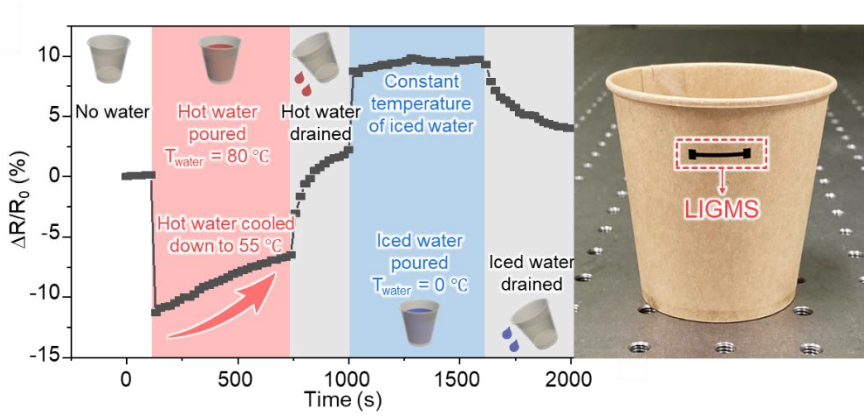

Figure 5.1: The real-life scenario of MPGS as beverage thermal sensor. To illustrate this, we conducted experiments on the response behavior of MPGS in detecting water temperature. The experiment involved pouring hot/cold water in a commercial paper cup, leaving it still for some time, and then draining it. The response of MPGS on the outer surface of the cup was recorded to determine the water temperature in real-time. A photograph showing MPGS on the outer surface of the commercial paper cup was included.

5.2 MPGS as food spoilage sensor in real-life scenario

In order to monitor the chemical status of food, the researchers used MPGS to measure the transient response of protein-rich foods such as raw pork meat and milk that were exposed to different thermal environments of refrigerated (approximately 4 ˚C) and warm state (approximately 37 ˚C). This process is demonstrated in **Figure 5.2**. To detect the spoilage level of raw pork meat, MPGS was placed on colored paper and placed inside a sealed container with the pork. It was then integrated into a wireless sensor module to deliver the spoilage level to the user's mobile phone in a visualized form, as shown in **Figure 5.2a(ii)**. The sensor resistance rapidly increases during the initial phase of spoilage, providing an indicator of food poisoning. However, there is no absolute quantitative indicator for the food poisoning level as the spoilage rate differs for each food product, depending on the type and mass of food products. In the warm condition, the rapid resistance surge in the initial stage indicates that the pork began to decompose and generate TMA gas over time (**Figure 5.2a(i)**). On the other hand, the relatively constant resistance change of the sensor in the refrigerated state implies that the pork remained fresh without any apparent implication of organic decomposition, which is also supported by a previous study [81]. The photographs of raw pork meat in the refrigerated and warm states at the end of the experiments are shown in **Figure 5.2a(iii)** and **(iv)**, respectively. These photos visually distinguish freshness by their appearances. The responses of both MPGS and the commercial gas sensor to

monitor the spoilage level of pork were compared in **Figure 5.3**, and the result corroborates that the gas sensing capability of MPGS exhibits sensitive performance similar to that of the commercial sensor.

Real-time monitoring of the milk spoilage level with MPGS showed a comparable outcome, where MPGS was in-situ fabricated on the inner surface of the milk carton, as demonstrated in **Figure 5.2b(ii)** and **(iii)**. As with the experiment with raw pork meat, the resistance of MPGS enclosed inside the carton with the milk in the warm oven gradually increased over time, whereas that of MPGS in the refrigerator remained unchanged. The snapshots in **Figure 5.2b(iii)** and **(iv)** visually capture a clear difference between the two samples, where the solid clots were visible for the sample preserved in the warm condition, while the control milk group remained visually unchanged. Regardless of the food state, solid or liquid, MPGS offers a potent solution to a wide range of ongoing problems, such as environmental and human health-related issues attributed to food poisoning, by developing a green-electronics platform for the user to recognize the food status before intake.

Both sets of findings demonstrated a notably heightened sensitivity when compared to the evaluation test conducted in Chapter 4.2. Unlike the controlled open environment of the evaluation test, which rigorously regulates the concentration of TMA gas, real-life scenarios represent closed environments where gas molecules accumulate within the package. Additionally,

the thermal and chemical signals of MPGS can be discerned despite both being detected through resistance shifts. In real-life scenarios, variations in temperature precede the occurrence of food spoilage reactions, thereby causing the resistance of MPGS to change initially in response to temperature fluctuations before becoming responsive to gas levels.

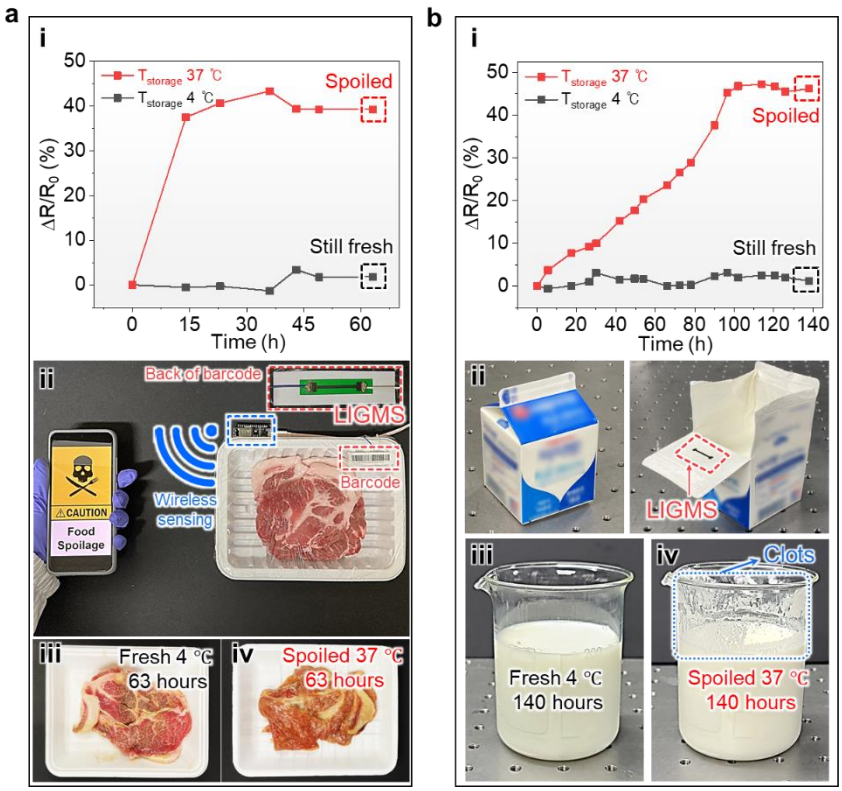

Figure 5.2: a) The practical application of MPGS is demonstrated in real-time monitoring of pork spoilage. (i) The response behavior of MPGS for detecting spoilage of pork stored at different temperatures (4 ˚C and 37 ˚C). (ii) A photograph of MPGS enclosed with the pork is provided. (iii, iv) Photographs of the pork preserved in the refrigerator and warm oven after 63 hours. The color change of

the spoiled pork belly at 37 ˚C after 63 hours is clearly evident when compared to that of the pork kept in the refrigerator. c) Another practical application of MPGS is the real-time wireless monitoring of milk spoilage. (i) The response behavior of MPGS for detecting spoilage of milk stored at different temperatures (4 ˚C and 37 ˚C). (ii) A milk carton purchased from a local market is used for the experiment, with MPGS in-situ patterned on the inner surface of the carton containing 200 mL of milk. (iii, iv) Photographs of the milk preserved in the refrigerator and warm oven after 140 hours are provided, showing solid clots which indicate the spoilage of milk at 37 ˚C.

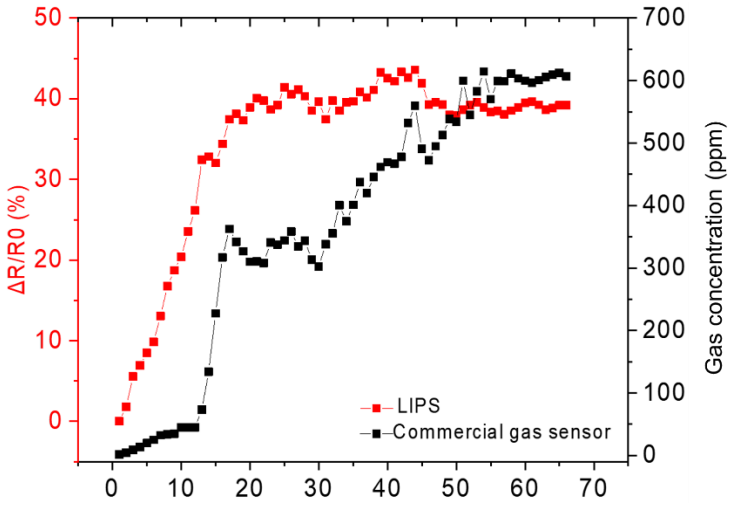

Figure 5.3: The change in resistance of MPGS and the commercial gas sensor when enclosed with the pork to monitor spoilage over time. The red line represents the data recorded by wireless monitoring with MPGS, while the black line represents data recorded by the commercial gas sensor.

Chapter 6

Conclusion and perspectives

To summarize, we transformed biodegradable commercial papers into a paper-based graphene electrode using laser processing to create MPGS, a device capable of monitoring the chemical and thermal status of food in real-time. The laser irradiation technique produced LIG on the commercial paper without harming the substrate, resulting in a decent sheet resistance of 105 Ω sq^{-1} at 100 mW and 10 mm s^{-1}. Our study also demonstrated that the LIG quality remained unaffected when switching between high-resolution and large-area patterning modes. Additionally, the all-in-one device/substrate architecture of MPGS eliminates the need for a separate sensor and paper substrate and can be applied to any commercial food packaging material with a simple laser patterning process. We also fabricated a biodegradable LIG circuit that can be customized and disposed of easily. The LIG sensor exhibited a temperature coefficient of resistance of -0.15 % $°C^{-1}$ and a gas coefficient of resistance of 0.0041% ppm^{-1}, indicating that two parameters can be decoupled based on magnitude and sign convention. The LIG gas sensor detected a broad range of gas concentrations, from 5 ppm to 40 ppm, making it capable of real-time detection of whether food is still edible or already spoiled. Finally, we developed a novel wireless monitoring system embedded in the biodegradable food packaging material that can

detect the real-time status of food without physically opening the package. We hope that our work will help prevent food poisoning and reduce non-biodegradable waste, as MPGS can monitor the present and future status of food products with chemical and thermo-sensing capabilities.

The development of green and biodegradable electronics is still in its early stages, mainly confined to laboratory research and yet to be implemented on an industrial or household level. However, there is a growing focus on sustainable electronics by various countries, institutions, corporations, and academics, which offers a positive outlook for the future. The green technology market is rapidly expanding due to the increased demand for environmental regulations, prompting major economies to invest in green electronics to promote their practical use. The research on green electronics has resulted in the creation of many materials with various practical applications. The authors predict that the use of fully green electronics will lead to a reduction in e-waste, making them ideal for low-cost disposable sensors with biodegradable features. As the technology matures and advances, green electronics will eventually become an integral part of our daily lives. While technological progress has brought both benefits and drawbacks to humanity, the authors believe that green electronics represent a step in the right direction and a solution to some of our current challenges.

Bibliography

(1) The World Bank. *Solid Waste Management*. 2022. https://www.worldbank.org/en/topic/urbandevelopment/brief/solid-waste-management (accessed March 22, 2023).

(2) The World Bank. *WHAT A WASTE 2.0*. https://datatopics.worldbank.org/what-a-waste/trends_in_solid_waste_management.html (accessed March 22, 2023).

(3) *It's time to shift to net-zero emissions plastics*. World Economic Forum, https://www.weforum.org/agenda/2022/01/it-s-time-to-shift-to-net-zero-emissions-plastics/ (accessed March 22, 2023).

(4) Post, T. W. *Drowning in garbage*. https://www.washingtonpost.com/graphics/2017/world/global-waste/ (accessed March 22, 2023).

(5) weeeforum. *International E-Waste Day: 57.4M Tonnes Expected in 2021*. https://weee-forum.org/ws_news/international-e-waste-day-2021/ (accessed September 20, 2022).

(6) Geneva Environment Network. *The Growing Environmental Risks of E-Waste*. 2023. https://www.genevaenvironmentnetwork.org/resources/updates/the-growing-environmental-risks-of-e-waste/ (accessed April 10, 2023).

(7) ScienceNews. *Earth's annual e-waste could grow to 75 million metric tons by 2030*. 2020. https://www.sciencenews.org/article/annual-e-waste-electronics-recycling-75-million-metric-tons (accessed April 10, 2022).

(8) Organization, W. H. *Food safety*. 2020. https://www.who.int/news-room/fact-sheets/detail/food-safety (accessed 2021 July 19th).

(9) Zheng, Y.; Yanful, E. K.; Bassi, A. S. A review of plastic waste biodegradation. *Critical reviews in biotechnology* **2005**, *25* (4), 243-250.

(10) Rawat, S. Food Spoilage: Microorganisms and their prevention. *Asian Journal of Plant Science and Research* **2015**, *5* (4), 47-56.

(11) Casalinuovo, I. A.; Di Pierro, D.; Coletta, M.; Di Francesco, P. Application of electronic noses for disease diagnosis and food spoilage detection. *Sensors* **2006**, *6* (11), 1428-1439.

(12) Loutfi, A.; Coradeschi, S.; Mani, G. K.; Shankar, P.; Rayappan, J. B. B. Electronic noses for food quality: A review. *Journal of Food Engineering* **2015**, *144*, 103-111.

(13) Yang, J.; Wei, D.; Tang, L.; Song, X.; Luo, W.; Chu, J.; Gao, T.; Shi, H.; Du, C. Wearable temperature sensor based on graphene nanowalls. *Rsc Advances* **2015**, *5* (32), 25609-25615.

(14) Yoon, H. J.; Yang, J. H.; Zhou, Z.; Yang, S. S.; Cheng, M. M.-C. Carbon dioxide gas sensor using a graphene sheet. *Sensors and Actuators B: Chemical* **2011**, *157* (1), 310-313.

(15) Choi, W.; Lahiri, I.; Seelaboyina, R.; Kang, Y. S. Synthesis of graphene and its applications: a review. *Critical Reviews in Solid State and Materials Sciences* **2010**, *35* (1), 52-71.

(16) Stankovich, S.; Dikin, D. A.; Piner, R. D.; Kohlhaas, K. A.; Kleinhammes, A.; Jia, Y.; Wu, Y.; Nguyen, S. T.; Ruoff, R. S. Synthesis of graphene-based nanosheets via chemical reduction of exfoliated graphite oxide. *carbon* **2007**, *45* (7), 1558-1565.
(17) Munoz, R.; Gómez-Aleixandre, C. Review of CVD synthesis of graphene. *Chemical Vapor Deposition* **2013**, *19* (10-11-12), 297-322.
(18) Stanford, M. G.; Yang, K.; Chyan, Y.; Kittrell, C.; Tour, J. M. Laser-induced graphene for flexible and embeddable gas sensors. *ACS nano* **2019**, *13* (3), 3474-3482.
(19) Stanford, M. G.; Li, J. T.; Chyan, Y.; Wang, Z.; Wang, W.; Tour, J. M. Laser-induced graphene triboelectric nanogenerators. *ACS nano* **2019**, *13* (6), 7166-7174.
(20) Ren, M.; Zhang, J.; Zhang, C.; Stanford, M. G.; Chyan, Y.; Yao, Y.; Tour, J. M. Quasi-solid-state Li–O2 batteries with laser-induced graphene cathode catalysts. *ACS Applied Energy Materials* **2020**, *3* (2), 1702-1709.
(21) Yan, Z.; Wang, L.; Xia, Y.; Qiu, R.; Liu, W.; Wu, M.; Zhu, Y.; Zhu, S.; Jia, C.; Zhu, M. Flexible High-Resolution Triboelectric Sensor Array Based on Patterned Laser-Induced Graphene for Self-Powered Real-Time Tactile Sensing. *Adv Funct Mater* **2021**, *31* (23), 2100709.
(22) Tao, L.-Q.; Tian, H.; Liu, Y.; Ju, Z.-Y.; Pang, Y.; Chen, Y.-Q.; Wang, D.-Y.; Tian, X.-G.; Yan, J.-C.; Deng, N.-Q. An intelligent artificial throat with sound-sensing ability based on laser induced graphene. *Nature communications* **2017**, *8* (1), 1-8.
(23) Marques, A. C.; Cardoso, A. R.; Martins, R.; Sales, M. G. F.; Fortunato, E. Laser-induced graphene-based platforms for dual biorecognition of molecules. *ACS Applied Nano Materials* **2020**, *3* (3), 2795-2803.
(24) Li, X.; Cai, W.; Teh, K. S.; Qi, M.; Zang, X.; Ding, X.; Cui, Y.; Xie, Y.; Wu, Y.; Ma, H. High-voltage flexible microsupercapacitors based on laser-induced graphene. *ACS applied materials & interfaces* **2018**, *10* (31), 26357-26364.
(25) Ye, R.; James, D. K.; Tour, J. M. Laser-induced graphene: from discovery to translation. *Advanced Materials* **2019**, *31* (1), 1803621.
(26) Lin, J.; Peng, Z.; Liu, Y.; Ruiz-Zepeda, F.; Ye, R.; Samuel, E. L.; Yacaman, M. J.; Yakobson, B. I.; Tour, J. M. Laser-induced porous graphene films from commercial polymers. *Nature communications* **2014**, *5* (1), 1-8.
(27) Le, T. S. D.; Park, S.; An, J.; Lee, P. S.; Kim, Y. J. Ultrafast laser pulses enable one-step graphene patterning on woods and leaves for green electronics. *Adv Funct Mater* **2019**, *29* (33), 1902771.
(28) Lu, L.; Yang, B.; Liu, J. Flexible multifunctional graphite nanosheet/electrospun-polyamide 66 nanocomposite sensor for ECG, strain, temperature and gas measurements. *Chem Eng J* **2020**, *400*, 125928.
(29) Nandy, S.; Goswami, S.; Marques, A.; Gaspar, D.; Grey, P.; Cunha, I.; Nunes, D.; Pimentel,

A.; Igreja, R.; Barquinha, P. Cellulose: a contribution for the zero e-waste challenge. *Advanced Materials Technologies* **2021**, *6* (7), 2000994.
(30) Cunha, I.; Barras, R.; Grey, P.; Gaspar, D.; Fortunato, E.; Martins, R.; Pereira, L. Reusable Cellulose-Based Hydrogel Sticker Film Applied as Gate Dielectric in Paper Electrolyte-Gated Transistors. *Adv Funct Mater* **2017**, *27* (16), 1606755.
(31) Lien, D.-H.; Kao, Z.-K.; Huang, T.-H.; Liao, Y.-C.; Lee, S.-C.; He, J.-H. All-printed paper memory. *ACS nano* **2014**, *8* (8), 7613-7619.
(32) Peng, Z.; Lin, J.; Ye, R.; Samuel, E. L.; Tour, J. M. Flexible and stackable laser-induced graphene supercapacitors. *ACS applied materials & interfaces* **2015**, *7* (5), 3414-3419.
(33) Clerici, F.; Fontana, M.; Bianco, S.; Serrapede, M.; Perrucci, F.; Ferrero, S.; Tresso, E.; Lamberti, A. In situ MoS2 decoration of laser-induced graphene as flexible supercapacitor electrodes. *ACS applied materials & interfaces* **2016**, *8* (16), 10459-10465.
(34) Zhang, J.; Zhang, C.; Sha, J.; Fei, H.; Li, Y.; Tour, J. M. Efficient water-splitting electrodes based on laser-induced graphene. *ACS applied materials & interfaces* **2017**, *9* (32), 26840-26847.
(35) Das, D.; Senapati, S.; Nanda, K. K. "Rinse, Repeat": an efficient and reusable SERS and catalytic platform fabricated by controlled deposition of silver nanoparticles on cellulose paper. *ACS Sustainable Chemistry & Engineering* **2019**, *7* (16), 14089-14101.
(36) Le, T. S. D.; Lee, Y. A.; Nam, H. K.; Jang, K. Y.; Yang, D.; Kim, B.; Yim, K.; Kim, S. W.; Yoon, H.; Kim, Y. J. Green Flexible Graphene–Inorganic-Hybrid Micro-Supercapacitors Made of Fallen Leaves Enabled by Ultrafast Laser Pulses. *Adv Funct Mater* **2021**, 2107768.
(37) Zheng, X.; Chen, W.; Wang, G.; Yu, Y.; Qin, S.; Fang, J.; Wang, F.; Zhang, X.-A. The Raman redshift of graphene impacted by gold nanoparticles. *AIP Advances* **2015**, *5* (5), 057133.
(38) Carvalho, A. F.; Fernandes, A. J.; Leitão, C.; Deuermeier, J.; Marques, A. C.; Martins, R.; Fortunato, E.; Costa, F. M. Laser-induced graphene strain sensors produced by ultraviolet irradiation of polyimide. *Adv Funct Mater* **2018**, *28* (52), 1805271.
(39) Kun, P.; Wéber, F.; Balázsi, C. Preparation and examination of multilayer graphene nanosheets by exfoliation of graphite in high efficient attritor mill. *Central European Journal of Chemistry* **2011**, *9* (1), 47-51.
(40) Chyan, Y.; Ye, R.; Li, Y.; Singh, S. P.; Arnusch, C. J.; Tour, J. M. Laser-induced graphene by multiple lasing: toward electronics on cloth, paper, and food. *ACS nano* **2018**, *12* (3), 2176-2183.
(41) Morant, C.; Andrey, J.; Prieto, P.; Mendiola, D.; Sanz, J.; Elizalde, E. XPS characterization of nitrogen-doped carbon nanotubes. *physica status solidi (a)* **2006**, *203* (6), 1069-1075.
(42) Tao, Z.; Du, J.; Qi, Z.; Ni, K.; Jiang, S.; Zhu, Y. Raman spectroscopy study of sp2 to sp3 transition in bilayer graphene under high pressures. *Appl Phys Lett* **2020**, *116* (13), 133101.
(43) Matindoust, S.; Farzi, A.; Nejad, M. B.; Abadi, M. H. S.; Zou, Z.; Zheng, L.-R. Ammonia gas sensor based on flexible polyaniline films for rapid detection of spoilage in protein-rich foods.

Journal of Materials Science: Materials in Electronics **2017**, *28* (11), 7760-7768.
(44) Shin, J.; Ko, J.; Jeong, S.; Won, P.; Lee, Y.; Kim, J.; Hong, S.; Jeon, N. L.; Ko, S. H. Monolithic digital patterning of polydimethylsiloxane with successive laser pyrolysis. *Nature Materials* **2021**, *20* (1), 100-107.
(45) Frank, O.; Mohr, M.; Maultzsch, J.; Thomsen, C.; Riaz, I.; Jalil, R.; Novoselov, K. S.; Tsoukleri, G.; Parthenios, J.; Papagelis, K. Raman 2D-band splitting in graphene: theory and experiment. *ACS nano* **2011**, *5* (3), 2231-2239.
(46) Dresselhaus, M.; Jorio, A.; Saito, R. Characterizing graphene, graphite, and carbon nanotubes by Raman spectroscopy. *Annu. Rev. Condens. Matter Phys.* **2010**, *1* (1), 89-108.
(47) Le, H. D.; Ngo, T. T. T.; Le, D. Q.; Nguyen, X. N.; Phan, N. M. Synthesis of multi-layer graphene films on copper tape by atmospheric pressure chemical vapor deposition method. *Advances in Natural Sciences: Nanoscience and Nanotechnology* **2013**, *4* (3), 035012.
(48) Cardoso, A. R.; Marques, A. C.; Santos, L.; Carvalho, A. F.; Costa, F. M.; Martins, R.; Sales, M. G. F.; Fortunato, E. Molecularly-imprinted chloramphenicol sensor with laser-induced graphene electrodes. *Biosensors and Bioelectronics* **2019**, *124*, 167-175.
(49) Yang, L.; Yi, N.; Zhu, J.; Cheng, Z.; Yin, X.; Zhang, X.; Zhu, H.; Cheng, H. Novel gas sensing platform based on a stretchable laser-induced graphene pattern with self-heating capabilities. *Journal of Materials Chemistry A* **2020**, *8* (14), 6487-6500.
(50) Ye, R.; Chyan, Y.; Zhang, J.; Li, Y.; Han, X.; Kittrell, C.; Tour, J. M. Laser-induced graphene formation on wood. *Advanced Materials* **2017**, *29* (37), 1702211.
(51) Luong, D. X.; Yang, K.; Yoon, J.; Singh, S. P.; Wang, T.; Arnusch, C. J.; Tour, J. M. Laser-induced graphene composites as multifunctional surfaces. *ACS nano* **2019**, *13* (2), 2579-2586.
(52) Li, J. T.; Stanford, M. G.; Chen, W.; Presutti, S. E.; Tour, J. M. Laminated laser-induced graphene composites. *ACS nano* **2020**, *14* (7), 7911-7919.
(53) Stanford, M. G.; Li, J. T.; Chen, Y.; McHugh, E. A.; Liopo, A.; Xiao, H.; Tour, J. M. Self-sterilizing laser-induced graphene bacterial air filter. *ACS nano* **2019**, *13* (10), 11912-11920.
(54) Stanford, M. G.; Zhang, C.; Fowlkes, J. D.; Hoffman, A.; Ivanov, I. N.; Rack, P. D.; Tour, J. M. High-resolution laser-induced graphene. Flexible electronics beyond the visible limit. *ACS Applied Materials & Interfaces* **2020**, *12* (9), 10902-10907.
(55) Garland, N. T.; McLamore, E. S.; Cavallaro, N. D.; Mendivelso-Perez, D.; Smith, E. A.; Jing, D.; Claussen, J. C. Flexible laser-induced graphene for nitrogen sensing in soil. *ACS applied materials & interfaces* **2018**, *10* (45), 39124-39133.
(56) Cao, L.; Zhu, S.; Pan, B.; Dai, X.; Zhao, W.; Liu, Y.; Xie, W.; Kuang, Y.; Liu, X. Stable and durable laser-induced graphene patterns embedded in polymer substrates. *Carbon* **2020**, *163*, 85-94.
(57) Zhang, Z.; Song, M.; Hao, J.; Wu, K.; Li, C.; Hu, C. Visible light laser-induced graphene

from phenolic resin: A new approach for directly writing graphene-based electrochemical devices on various substrates. *Carbon* **2018**, *127*, 287-296.
(58) Han, X.; Ye, R.; Chyan, Y.; Wang, T.; Zhang, C.; Shi, L.; Zhang, T.; Zhao, Y.; Tour, J. M. Laser-induced graphene from wood impregnated with metal salts and use in electrocatalysis. *ACS Applied Nano Materials* **2018**, *1* (9), 5053-5061.
(59) Bobinger, M. R.; Romero, F. J.; Salinas-Castillo, A.; Becherer, M.; Lugli, P.; Morales, D. P.; Rodríguez, N.; Rivadeneyra, A. Flexible and robust laser-induced graphene heaters photothermally scribed on bare polyimide substrates. *Carbon* **2019**, *144*, 116-126.
(60) Nasser, J.; Lin, J.; Zhang, L.; Sodano, H. A. Laser induced graphene printing of spatially controlled super-hydrophobic/hydrophilic surfaces. *Carbon* **2020**, *162*, 570-578.
(61) Rajan, G.; Morgan, J. J.; Murphy, C.; Torres Alonso, E.; Wade, J.; Ott, A. K.; Russo, S.; Alves, H.; Craciun, M. F.; Neves, A. I. Low operating voltage carbon–graphene hybrid E-textile for temperature sensing. *ACS Applied Materials & Interfaces* **2020**, *12* (26), 29861-29867.
(62) Ji, X.; Wang, H.; Chen, T.; Zhang, T.; Chu, J.; Du, A. Intrinsic negative TCR of superblack carbon aerogel films and their ultrabroad band response from UV to microwave. *Carbon* **2020**, *161*, 590-598.
(63) Dinh, T.; Phan, H.-P.; Dao, D. V.; Woodfield, P.; Qamar, A.; Nguyen, N.-T. Graphite on paper as material for sensitive thermoresistive sensors. *Journal of Materials Chemistry C* **2015**, *3* (34), 8776-8779.
(64) Sahatiya, P.; Puttapati, S. K.; Srikanth, V. V.; Badhulika, S. Graphene-based wearable temperature sensor and infrared photodetector on a flexible polyimide substrate. *Flexible and Printed Electronics* **2016**, *1* (2), 025006.
(65) Cui, X.; Chen, J.; Zhu, Y.; Jiang, W. Lightweight and conductive carbon black/chlorinated poly (propylene carbonate) foams with a remarkable negative temperature coefficient effect of resistance for temperature sensor applications. *Journal of Materials Chemistry C* **2018**, *6* (35), 9354-9362.
(66) Shin, J.; Jeong, B.; Kim, J.; Nam, V. B.; Yoon, Y.; Jung, J.; Hong, S.; Lee, H.; Eom, H.; Yeo, J. Sensitive wearable temperature sensor with seamless monolithic integration. *Advanced Materials* **2020**, *32* (2), 1905527.
(67) Bang, J.; Lee, W. S.; Park, B.; Joh, H.; Woo, H. K.; Jeon, S.; Ahn, J.; Jeong, C.; Kim, T. i.; Oh, S. J. Highly Sensitive Temperature Sensor: Ligand-Treated Ag Nanocrystal Thin Films on PDMS with Thermal Expansion Strategy. *Adv Funct Mater* **2019**, *29* (32), 1903047.
(68) Choi, H.; Choi, J. S.; Kim, J. S.; Choe, J. H.; Chung, K. H.; Shin, J. W.; Kim, J. T.; Youn, D. H.; Kim, K. C.; Lee, J. I. Flexible and transparent gas molecule sensor integrated with sensing and heating graphene layers. *Small* **2014**, *10* (18), 3685-3691.
(69) Seekaew, Y.; Lokavee, S.; Phokharatkul, D.; Wisitsoraat, A.; Kerdcharoen, T.; Wongchoosuk,

C. Low-cost and flexible printed graphene–PEDOT: PSS gas sensor for ammonia detection. *Organic Electronics* **2014**, *15* (11), 2971-2981.
(70) Zhao, Y.; Song, J.-G.; Ryu, G. H.; Ko, K. Y.; Woo, W. J.; Kim, Y.; Kim, D.; Lim, J. H.; Lee, S.; Lee, Z. Low-temperature synthesis of 2D MoS 2 on a plastic substrate for a flexible gas sensor. *Nanoscale* **2018**, *10* (19), 9338-9345.
(71) Kim, J.-W.; Porte, Y.; Ko, K. Y.; Kim, H.; Myoung, J.-M. Micropatternable double-faced ZnO nanoflowers for flexible gas sensor. *ACS applied materials & interfaces* **2017**, *9* (38), 32876-32886.
(72) He, Q.; Zeng, Z.; Yin, Z.; Li, H.; Wu, S.; Huang, X.; Zhang, H. Fabrication of flexible MoS2 thin-film transistor arrays for practical gas-sensing applications. *Small* **2012**, *8* (19), 2994-2999.
(73) Zhang, Z.; Zou, X.; Xu, L.; Liao, L.; Liu, W.; Ho, J.; Xiao, X.; Jiang, C.; Li, J. Hydrogen gas sensor based on metal oxide nanoparticles decorated graphene transistor. *Nanoscale* **2015**, *7* (22), 10078-10084.
(74) Kim, H. W.; Na, H. G.; Kwon, Y. J.; Kang, S. Y.; Choi, M. S.; Bang, J. H.; Wu, P.; Kim, S. S. Microwave-assisted synthesis of graphene–SnO2 nanocomposites and their applications in gas sensors. *ACS applied materials & interfaces* **2017**, *9* (37), 31667-31682.
(75) Chen, Z.; Umar, A.; Wang, S.; Wang, Y.; Tian, T.; Shang, Y.; Fan, Y.; Qi, Q.; Xu, D.; Jiang, L. Supramolecular fabrication of multilevel graphene-based gas sensors with high NO 2 sensibility. *Nanoscale* **2015**, *7* (22), 10259-10266.
(76) Jiang, G.; Goledzinowski, M.; Comeau, F. J.; Zarrin, H.; Lui, G.; Lenos, J.; Veileux, A.; Liu, G.; Zhang, J.; Hemmati, S. Free-standing functionalized graphene oxide solid electrolytes in electrochemical gas sensors. *Adv Funct Mater* **2016**, *26* (11), 1729-1736.
(77) Long, H.; Harley-Trochimczyk, A.; Pham, T.; Tang, Z.; Shi, T.; Zettl, A.; Carraro, C.; Worsley, M. A.; Maboudian, R. High surface area MoS2/graphene hybrid aerogel for ultrasensitive NO2 detection. *Adv Funct Mater* **2016**, *26* (28), 5158-5165.
(78) Qin, J.; Gao, J.; Shi, X.; Chang, J.; Dong, Y.; Zheng, S.; Wang, X.; Feng, L.; Wu, Z. S. Hierarchical ordered dual-mesoporous polypyrrole/graphene nanosheets as bi-functional active materials for high-performance planar integrated system of micro-supercapacitor and gas sensor. *Adv Funct Mater* **2020**, *30* (16), 1909756.
(79) Luo, G.; Xie, L.; He, M.; Jaisutti, R.; Zhu, Z. Flexible fabric gas sensors based on reduced graphene-polyaniline nanocomposite for highly sensitive NH 3 detection at room temperature. *Nanotechnology* **2021**, *32* (30), 305501.
(80) Huang, S.; Panes-Ruiz, L. A.; Croy, A.; Löffler, M.; Khavrus, V.; Bezugly, V.; Cuniberti, G. Highly sensitive room temperature ammonia gas sensor using pristine graphene: The role of biocompatible stabilizer. *Carbon* **2021**, *173*, 262-270.
(81) Cai, C.; Mo, J.; Lu, Y.; Zhang, N.; Wu, Z.; Wang, S.; Nie, S. Integration of a porous wood-

based triboelectric nanogenerator and gas sensor for real-time wireless food-quality assessment. *Nano Energy* **2021**, *83*, 105833.

초록

세계적인 폐기물 문제인 플라스틱 폐기물과 전자 폐기물을 포함하여 심각해지면서 전자 제품에서 더욱 친환경적인 재료의 필요성이 커지고 있다. 따라서, 식품 포장용 생분해성 재료의 사용과 식품 품질의 실시간 모니터링은 폐기물 문제와 인간 건강 관리에 있어서 중요하다. 최첨단 그래핀 합성 방법인 레이저 유도 그래핀(LIG)은 우수한 특성과 공정의 실행 가능성으로 인해 폭넓게 연구되었다. 본 논문에서는 LIG-on-paper 생분해성 기판을 기반으로 한 멀티모달 종이 그래핀 센서(MPGS)를 제안하여 차세대 친환경 전자 제품을 개발한다. 연속 파동 레이저의 직접 조사는 다양한 종이 기판에 LIG 를 형성하여 우수한 면저항 (105 Ω/sq-1)을 갖게 한다. 또한, LIG-on-paper 의 다공성 구조는 외부 자극에 민감하게 반응하도록 하여 센서로의 응용에 유용하다. 따라서, LIG-on-paper 는 단일 전극을 통해 온도와 트리메틸아민(TMA) 가스에 대하여 각각 0.15%°C-1 및 0.0041%ppm-1 의 감도를 가져 온도-가스 멀티모달 센서로 적용되었다. 개념 검증을 위해, 우리는 음식의 온도와 변질 가스를 동시에 감지하는 스마트 식품 관리 시스템을 개발하였다. 임베디드 프로세서의 무선 통신을 통해 수신된 데이터는 즉시 모바일 장치로 전송될 수 있다. 우리는 이 종이 기반 전자 제품 연구가 전 세계적인 폐기물과 식품 안전 문제에 대한 차세대 친환경 전자 제품 발전을 이끌어낼 것이라 믿는다.

주요어 : 레이저 유도 그래핀, 멀티모달 종이 그래핀 센서, 친환경 물질, 식품 부패, 연속광 레이저, 스마트 식품 관리

학 번 : 2017-23145